Available online at www.sciencedirect.com
SCIENCE DIRECT®
Journal of Sound and Vibration 274 (2004) 893–914
JOURNAL OF SOUND AND VIBRATION
www.elsevier.com/locate/jsvi

Effect of high-frequency low-amplitude vibration on the performance of a class of semi-active base isolation systems with on–off damping

S. Chatterjee*, T.K. Singha, S.K. Karmakar

Department of Mechanical Engineering, Bengal Engineering College (Deemed University), P.O. Botanic Garden, Howrah 711103, West Bengal, India

Received 21 August 2002; accepted 23 May 2003

Abstract

An alternative vibration isolator that incorporates on–off friction damper with fast excitation input at the base of the damper is proposed in this paper. Friction is modelled using the Coulomb's friction model as well as the LuGre model. Analytical expressions are obtained for the effective damper performance under fast excitation, and the performance of the isolator is studied in light of the effective damping characteristics. Numerical simulation of equation of motion validates the analytical results.

1. Introduction

Passive vibration isolators are the most simple, inexpensive and reliable means of protecting sensitive equipment from environmental shock and vibration. However, passive isolators are seriously limited in performance due to fixed parameters values, specifically fixed damping. In passive isolators with fixed damping parameter, transmissibility characteristics cannot be favourably controlled over a wide range of frequencies by increasing or decreasing damping value. Research on this topic has established that isolators perform far better with variable damping or stiffness. Damping and stiffness can be varied either in active or semi-active manner. However, due to low energy consumption, semi-active isolators are more attractive in practice.

Possibly, the first significant contribution on semi-active isolator is done by Karnoop et al. [1,2]. They have shown that when one end of the damper of an isolator is grounded, i.e., the damper

*Corresponding author.
E-mail address: shy@mech.becs.ac.in (S. Chatterjee).

0022-460X/$ - see front matter © 2003 Elsevier Ltd. All rights reserved.
doi:10.1016/S0022-460X(03)00651-5

force always acts against the absolute velocity of the isolated mass, isolator performance improves remarkably, and this also circumvents the non-uniform effect of damping on transmissibility characteristics. Such configuration is known as the sky-hook damping. Clearly, an inertial frame of reference is required for hardware realization of the sky-hook damping, which is practically impossible in most of the situations. Karnoop et al. propose a semi-active control technique to emulate sky-hook damping, where depending on the sign of a predefined switch function, the damper is electro-mechanically modulated to generate the highest and the lowest possible values of damping. The switch function proposed by them is the product of the absolute and relative velocities of the mass, and the damper is modulated to produce high damping when the sign of this switch function is positive. By this arrangement, damping force either acts against the absolute velocity of the mass or becomes zero. Rakheja and Sankar [3] propose a similar on–off control of the damper based on a switch function involving relative displacement and velocity of the isolated mass. With the advent of smart fluids, like MR and ER fluids, the hardware realization of semi-active on–off control [4,5] has become much simpler, and this has found wider applications.

Although isolators based on fluidic dampers have a wide range of applications, these are largely unsuitable for space and other applications. Friction damping has been proved to be suitable in such situations [6]. Yamaguchi et al. [7] consider variable stiffness control of spring using friction joint for vibration isolation. Nishitani et al. [8] consider variable friction damper for vibration isolation systems.

In the present paper, an alternative vibration isolation system is proposed. The damper of the isolator is a variable friction damper, where the friction force is changed by semi-actively controlling the normal force on the friction joint of the damper. The rigid base of the friction damper is subjected to a very high frequency low-amplitude vibration. The friction damper is modelled using the steady state Coulomb's friction model as well as the LuGre [9] dynamic friction model. Mathematical models are developed, and theoretical analysis is performed using the method of direct partition of motion (MDPM) of the theory of fast vibration [10] and the singular perturbation theory [11]. Performance of the isolator is studied both analytically and numerically. It has been shown that the effective damping characteristics of the damper are favourably modified due to the application of high-frequency vibration. In this context, it is worthwhile referring to literature related to the effect of high-frequency vibration (so-called fast vibration) on non-linear systems. Recent research has established that fast vibration has non-trivial effect on the damping [12], elastic stiffness [13], as well as dynamic behaviour [14–16] of a variety of non-linear systems. These effects are known as the fast-vibration phenomena, and have found wide practical applications [17–19].

2. Mathematical model

The mathematical model of a single-degree-of-freedom base isolation system with base excitation X_e^*, and deliberately introduced fast excitation X_f^* is depicted in Fig. 1. The damper in the model is a semi-active friction damper. The normal force on the friction damper is varied according to the following rule:

$$F_n(X^{*'}, X_e^{*'}, X_f^{*'}) = N|X^{*'} - X_e^{*'} - X_f^{*'}|\mathrm{U}[X'^{*}(X^{*'} - X_e^{*'} - X_f^{*'})], \tag{1}$$

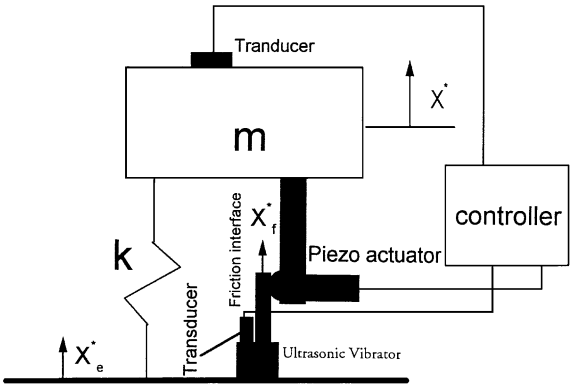

Fig. 1. Mathematical model of the system under consideration.

where prime ($'$) denotes differentiation with respect to time t. U(.) is the Heaviside step function and N is controller gain.

The equation of motion of the system shown in Fig. 1 is written as

$$mX''^* + \mu F_n \operatorname{sgn}(X'^* - X_e'^* - X_f'^*) + k(X^* - X_e^*) = 0, \tag{2}$$

where μ is the coefficient of friction of the friction damper.

A non-dimensional form of Eq. (2) is as follows:

$$\ddot{X} + h(\dot{X} - \dot{X}_e - \dot{X}_f)S + X - X_e = 0, \tag{3}$$

where the switching function S is written as

$$S = \mathrm{U}\{\dot{X}(\dot{X} - \dot{X}_e - \dot{X}_f)\}. \tag{4}$$

The non-dimensional quantities are defined below:

$$\ddot{X} = \frac{X^{*''}}{\omega_n^2 x_0}, \quad \dot{X} = \frac{X^{*'}}{\omega_n x_0}, \quad X = \frac{X^*}{x_0}, \qquad \omega_n = \sqrt{\frac{k}{m}}, \qquad h = \frac{\mu N}{m\omega_n},$$

$$X_e = \frac{X_e^*}{x_0}, \quad \dot{X}_e = \frac{X_e^{*'}}{\omega_n x_0}, \quad X_e = \frac{X_e^*}{x_0}, \quad \dot{X}_e = \frac{X_e^{*'}}{\omega_n x_0}, \quad X_f = \frac{X_f^*}{x_0}, \quad \dot{X}_f = \frac{X_f^{*'}}{\omega_n x_0},$$

and x_0 is the amplitude of base excitation. The 'dot' denotes differentiation with respect to the non-dimensional time $\tau = t\omega_n$.

3. Theoretical analysis

3.1. Harmonic fast excitation

When fast excitation is assumed to be harmonic, i.e.,

$$X_f^* = A_f \sin(\Omega_f t),$$

$$X_f = q\sin(\Omega\tau) \quad \text{with } \Omega = \frac{\Omega_f}{\omega_n} \text{ and } q = \frac{A_f}{x_0}, \tag{5}$$

equation of motion takes the following form:

$$\ddot{X} + h(\dot{X} - \dot{X}_e - q\Omega\cos(\Omega\tau))S + X - X_e = 0, \tag{6}$$

where

$$S = \mathrm{U}\{\dot{X}(\dot{X} - \dot{X}_e - q\Omega\cos(\Omega\tau))\}. \tag{7}$$

One should note here that $\Omega \gg 1$ and $q \ll 1$, such that $q\Omega \sim O(1)$.

Putting $Y = X - X_e - q\sin(\Omega\tau)$, one can rewrite Eq. (6) as

$$\ddot{Y} + h\dot{Y}S_0 + Y = -\ddot{X}_e + q\Omega^2\sin(\Omega\tau) - q\sin(\Omega\tau), \tag{8}$$

where

$$S_0 = \mathrm{U}\{(\dot{Y} + \dot{X}_e + q\Omega\cos(\Omega\tau))\dot{Y}\}. \tag{9}$$

According to the MDPM [10], the displacement variable Y may be split into slow (Z) and fast (ϕ) components as follows:

$$Y = Z + \Omega^{-1}\phi(\tau, \Omega\tau). \tag{10}$$

Therefore,

$$\dot{Y} = \dot{Z} + \phi'' + \Omega^{-1}\dot{\phi} \tag{11}$$

and

$$\ddot{Y} = \ddot{Z} + \phi''\Omega + 2\dot{\phi}' + \Omega^{-1}\ddot{\phi}, \tag{12}$$

where prime ($'$) and dot ($\dot{}$) denotes differentiation with respect to T and τ, respectively, and fast time average of $\phi(\tau, \Omega\tau)$ is zero, i.e.,

$$\langle\phi\rangle = \frac{1}{2\pi}\int_0^{2\pi}\phi(\tau, \Omega\tau)\,\mathrm{d}(\Omega\tau) = 0. \tag{13}$$

Putting Eqs. (10)–(12) into Eqs. (6) and (7), one obtains

$$\phi'' = -\Omega^{-1}\{\ddot{Z} + 2\dot{\phi}' + h(\dot{Z} + \phi')S_f + Z + \ddot{X}_e\} + q\Omega\sin(\Omega\tau) + O(\Omega^{-2}) = 0, \tag{14}$$

where

$$S_f = \mathrm{U}[(\dot{Z} + \phi' + \dot{X}_e + q\Omega\cos(\Omega\tau))(\dot{Z} + \phi')]. \tag{15}$$

The first order form of Eq. (14) is given by

$$\phi'' = q\Omega\sin(\Omega\tau). \tag{16}$$

Therefore, the first order solution of Eq. (14) may be written as

$$\phi' = -q\Omega\cos(\Omega\tau), \tag{17}$$

and

$$\phi = -q\Omega\sin(\Omega\tau). \tag{18}$$

Thus, using Eq. (13) one can take average of Eq. (14) to obtain the slow dynamics of the system as given below:

$$\ddot{Z} + h\langle D\rangle + Z = -\ddot{X}_e, \tag{19}$$

where

$$\langle D\rangle = \frac{1}{2\pi}\int_0^{2\pi} (\dot{Z} - q\Omega\cos\theta)\mathrm{U}[\{\dot{Z} + \dot{X}_e\}\{\dot{Z} - q\Omega\cos\theta\}]\,\mathrm{d}\theta. \tag{20}$$

The average damping function $\langle D\rangle$ given by Eq. (20) is expressed as (see the appendix for details)

$$\langle D\rangle = \begin{cases} (\dot{X} - \dot{X}_e) + \dfrac{1}{\pi}\left\{q\Omega\sin\theta_1 - \cos^{-1}\left(\dfrac{\dot{X} - \dot{X}_e}{q\Omega}\right)(\dot{X} - \dot{X}_e)\right\}, & \forall \dot{X} > 0 \text{ and } |\dot{X} - \dot{X}_e| \leqslant q\Omega, \\ \dfrac{1}{\pi}\left\{\cos^{-1}\left(\dfrac{\dot{X} - \dot{X}_e}{q\Omega}\right)(\dot{X} - \dot{X}_e) - q\Omega\sin\theta_1\right\}, & \forall \dot{X} < 0 \text{ and } |\dot{X} - \dot{X}_e| \leqslant q\Omega, \\ \dot{X} - \dot{X}_e, & \forall \dot{X} \text{ and } |\dot{X} - \dot{X}_e| \leqslant q\Omega, \\ 0 & \text{otherwise.} \end{cases} \tag{21}$$

Finally, one obtains the equation of motion governing the average low-frequency dynamics of the system as

$$\ddot{X} + h\langle D\rangle + (X - X_e) = 0, \tag{22}$$

where $\langle D\rangle$ is as described in Eq. (21). Eq. (22) is obviously a non-linear differential equation, and it is not easy to solve this equation. However, by looking into the nature of the effective damping function $\langle D\rangle$, one can extract important information regarding the performance of the isolation system. As an example, graphical natures of the effective damping function with and without fast excitation are shown in Figs. 2(a) and (b), respectively. It is to be noted that the

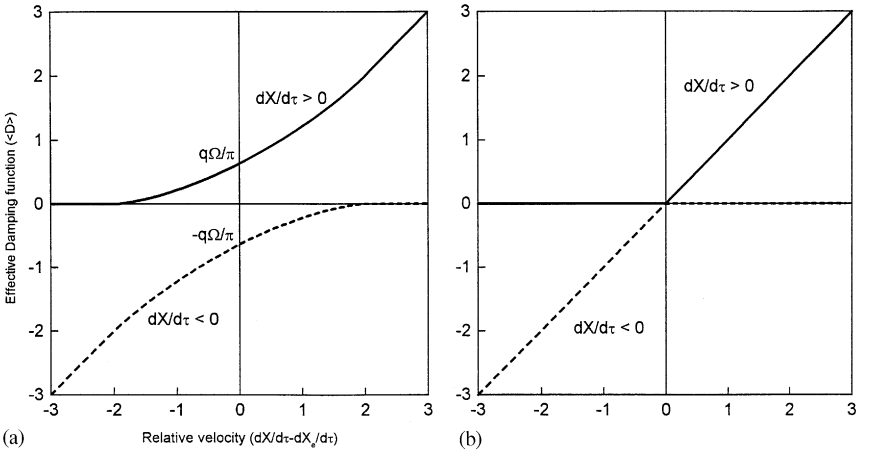

Fig. 2. Effective damping function vs. relative velocity: ——, positive absolute velocity; -----, negative absolute velocity. $q\Omega = 2$. (a) With fast excitation; (b) without fast excitation.

damper is controlled in on–off fashion depending on the sign of the product of the absolute velocity of the mass and the relative velocity across the damper. Therefore, for a particular value of relative velocity across the damper, the damper produces either zero or some non-trivial force depending on the sign of the absolute velocity of the mass. In semi-active sky-hook control without fast excitation, as shown in Fig. 2(b), the damper turns off when the product of the absolute and relative velocity are of opposite signs. This is because of the fact that under such circumstances, the damper force acts in the direction of the absolute velocity of the mass, and thereby tends to destabilize the system by instilling energy into it. However, it is observed from Fig. 2(a) that in presence of fast excitation, the effective damping force may still act against the absolute velocity of the mass (at least for some time) under the same circumstances. Moreover, in presence of high-frequency excitation, overall low-velocity ($<q\Omega$) damping of the system is also improved (zero velocity damping is $q\Omega/\pi$). Therefore, the damper with fast excitation emulates the ideal sky-hook damping more closely, and under such circumstances, one obviously expects better isolation characteristics. The detailed discussion of the isolator performance is presented elsewhere in the paper.

3.2. Triangular fast excitation

It is observed in the previous section that when sinusoidal fast excitation is used, the problem is not amenable to analytical solutions. However, it is understood that the closed form analytical solutions are possible for fast excitation having triangular pulse waveform. The shape of the waveform of the fast excitation is depicted in Fig. 3, and has a non-dimensional amplitude q and time period T_0. Therefore, the magnitude of the velocity amplitude of the fast excitation is given by

$$V = \frac{4q}{T_0}. \tag{23}$$

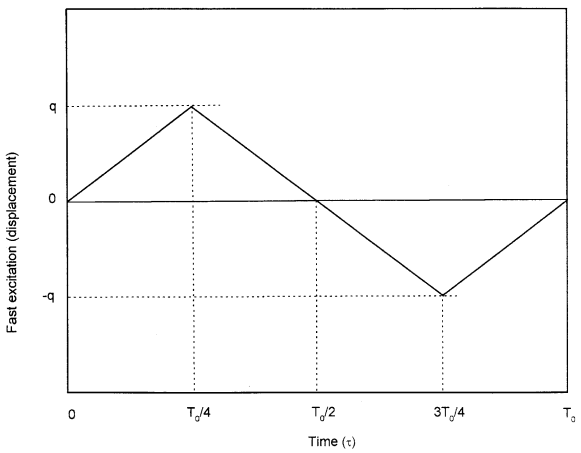

Fig. 3. Triangular fast excitation.

In that case, the effective damping function $\langle D \rangle$ in Eq. (19) is expressed as

$$\langle D \rangle = \frac{(\dot{Z}+V)*\mathrm{U}[(\dot{Z}+\dot{X}_e)(\dot{Z}+V)] + (\dot{Z}-V)*\mathrm{U}[(\dot{Z}+\dot{X}_e)(\dot{Z}-V)]}{2}. \tag{24}$$

The general shape of $\langle D \rangle$ is illustrated in Fig. 4. From Fig. 4, it is observed that the effective damping $\langle D \rangle$ is a piecewise linear function, and this renders Eq. (19) solvable in the closed form. In what follows, the method of solution for single-harmonic base excitation is described in detail.

Two different types of solutions are possible as listed below:

(1) $|\dot{Z}| > V$, Fig. 5(a),
(2) $|\dot{Z}| < V$, Fig. 5(b).

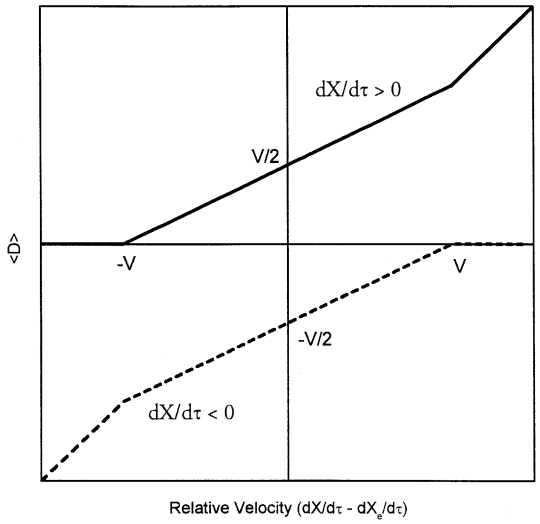

Fig. 4. The general shape of the effective damping function $\langle D \rangle$ for triangular fast excitation: ——, positive absolute velocity; - - - - -, negative absolute velocity.

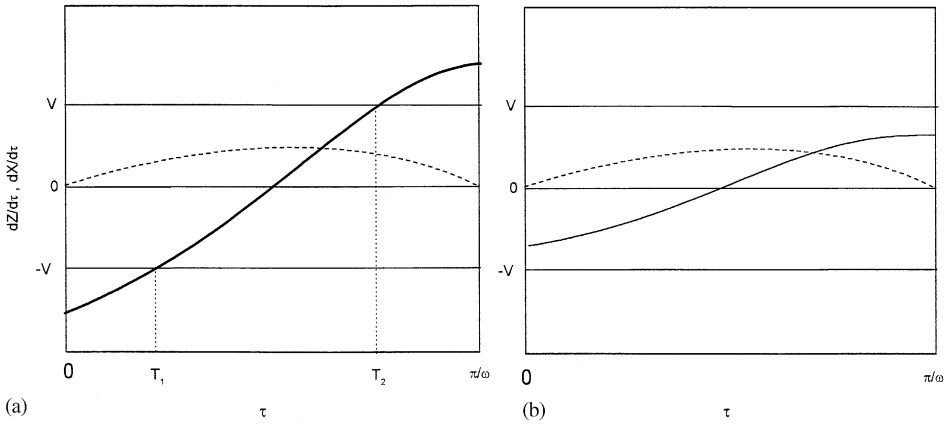

Fig. 5. Types of solutions under consideration: ——, $\mathrm{d}Z/\mathrm{d}\tau$; - - - - -, $\mathrm{d}X/\mathrm{d}\tau$.

Case (1): In this case, one can split Eq. (19) into following three linear equations, each valid for a particular time interval:

$$\left.\begin{aligned} &Z = Z_1, \quad \ddot{Z}_1 + Z_1 = \omega^2 \sin(\omega\tau + \varphi) \qquad \forall 0 < \tau \leqslant T_1 \\ &Z = Z_2, \quad \ddot{Z}_2 + \frac{h}{2}(\dot{Z}_2 + V) + Z_2 = \omega^2 \sin(\omega\tau + \varphi) \qquad \forall T_1 \leqslant \tau \leqslant T_2 \\ &Z = Z_3, \quad \ddot{Z}_3 + h\dot{Z}_3 + Z_3 = \omega^2 \sin(\omega\tau + \varphi) \qquad \forall T_2 \leqslant \tau \leqslant \pi/\omega \end{aligned}\right\} \quad \forall \dot{Z} + \dot{X}_e \geqslant 0, \quad (25)$$

where

$$X_e = \sin(\omega\tau).$$

The solution being symmetric, only a single half of the time period is considered. To adjust the arbitrary setting of the time origin, an unknown phase φ is introduced. Now one can express the solutions of Eq. (25) as given below:

$$Z_1 = d_1 \cos(\eta_1\tau) + d_2 \sin(\eta_1\tau) + M_1 \sin(\omega\tau + \varphi), \quad (26)$$

where

$$M_1 = \frac{\omega^2}{1 - \omega^2} \quad \text{and} \quad \eta_1 = 1.$$

$$Z_2 = \mathrm{e}^{-\lambda(\tau - T_1)}[d_3 \cos(\eta_2(\tau - T_2)) + d_4 \sin(\eta_2(\tau - T_2))] + M_2 \sin(\omega\tau + \varphi + \theta_2) - \frac{Vh}{2}, \quad (27)$$

where

$$\lambda = \frac{h}{4}, \quad M_2 = \frac{\omega^2}{\sqrt{(1 - \omega^2)^2 + (0.5h\omega)^2}}, \quad \theta_2 = \tan^{-1}\left(\frac{-0.5h\omega}{1 - \omega^2}\right), \quad \eta_2 = \sqrt{1 - \lambda^2}.$$

$$Z_3 = \mathrm{e}^{-2\lambda(\tau - T_2)}[d_5 \cos(\eta_3(\tau - T_2)) + d_6 \sin(\eta_3(\tau - T_2))] + M_3 \sin(\omega\tau + \varphi + \theta_3), \quad (28)$$

where

$$M_3 = \frac{\omega^2}{\sqrt{(1 - \omega^2)^2 + (h\omega)^2}}, \quad \theta_3 = \tan^{-1}\left(\frac{-h\omega}{1 - \omega^2}\right), \quad \eta_3 = \sqrt{1 - \left(\frac{h}{2}\right)^2}.$$

In Eqs. (26)–(28), d_i $(i = 1, \ldots, 6)$ are unknown constants which can be evaluated as described below. Considering the continuity, C^1 smoothness, symmetry and periodicity of the solution, one can write the following nine relationships between the three segments of the solution:

$$\dot{Z}_1(T_1) = \dot{Z}_2(T_1) = -V,$$

$$Z_1(T_1) = Z_2(T_1),$$

$$Z_2(T_2) = Z_3(T_2),$$

$$\dot{Z}_2(T_2) = \dot{Z}_3(T_2),$$

$$Z_1(0) = -Z_3\left(\frac{\pi}{\omega}\right),$$

$$\dot{Z}_1(0) = -\omega\cos\varphi,$$

$$\dot{Z}_3\left(\frac{\pi}{\omega}\right) = \omega\cos\varphi. \tag{29}$$

Using Eqs. (29), one finds nine equations for nine unknowns, namely d_i $(i = 1, \ldots, 6)$, and φ, T_1, T_2. However, a closer look shows that d_i $(i = 1, \ldots, 6)$ can be explicitly expressed as functions of φ, T_1, T_2, through the following equation:

$$[A]\{d\} = \{b\}, \tag{30}$$

where

$$[A] = \begin{bmatrix} -\eta_1\sin(\eta_1 T_1) & \eta_1\cos(\eta_1 T_1) & 0 & 0 & 0 & 0 \\ 0 & 0 & -\lambda & \eta_2 & 0 & 0 \\ \cos(\eta_1 T_1) & \sin(\eta_1 T_1) & -1 & 0 & 0 & 0 \\ 0 & 0 & 0 & 0 & -2\lambda & \eta_3 \\ 1 & 0 & 0 & 0 & \mathrm{e}^{-2\lambda T_d}\cos(\eta_3 T_d) & \mathrm{e}^{-2\lambda T_d}\sin(\eta_3 T_d) \\ 0 & \eta_1 & 0 & 0 & 0 & 0 \end{bmatrix},$$

with

$$T_d = \frac{\pi}{\omega} - T_2,$$

$$\{d\} = \{d_1 \;\; d_2 \;\; d_3 \;\; d_4 \;\; d_5 \;\; d_6\}^{\mathrm{T}},$$

and

$$\{b\} = \begin{Bmatrix} -M_1\omega\cos(\omega T_1 + \varphi) - V \\ -M_2\omega\cos(\omega T_1 + \varphi + \theta_2) - V \\ -M_1\sin(\omega T_1 + \varphi) + M_2\sin(\omega T_1 + \varphi + \theta_2) - Vh/2 \\ V - M_3\omega\cos(\omega T_2 + \varphi + \theta_3) \\ M_3\sin(\varphi + \theta_3) - M_1\sin\varphi \\ -(M_1 + 1)\omega\cos\varphi \end{Bmatrix}.$$

Thus, one is left with only three non-linear algebraic equations in three unknowns, which can be solved, and back-substituted to express the solution of Eq. (19) as

$$Z(\tau) = Z_1 + (Z_2 - Z_1)\mathrm{U}(\tau - T_1) + (Z_3 - Z_2 - Z_1)\mathrm{U}(\tau - T_2). \tag{31}$$

Finally, $X(\tau)$ is obtained as $X(\tau) = Z(\tau) + X_e$.

Case (2): In this case, one simply considers the segment Z_2, and proceeds in the similar fashion. Stability of the solutions thus obtained can be ascertained using the method of error propagation [20].

3.3. Numerical results and discussions

In Sections 3.1 and 3.2, the effective damping functions are constructed analytically for single-harmonic and triangular fast excitation. It is understood that in presence of fast excitation, the effective damping function emulates the ideal sky-hook damping in a much better way, and as a

consequence one expects better transmissibility characteristics compared to that obtained from ordinary on–off damping. In the present section, a detailed study of the performance of on–off dampers with fast excitation is carried out. The displacement transmissibility is taken as the performance index. It is to be noted that if base excitation is taken as $X_e^* = x_0 \sin(\omega_e t)$, non-dimensional base excitation becomes $X_e = \sin(\omega\tau)$, where $\omega = \omega_e/\omega_n$. Then displacement transmissibility is equivalent to X.

It is discussed in Section 3.2 that analytical solutions of the transmissibility characteristics are difficult to obtain for harmonic fast excitation. Therefore, numerical solutions of Eq. (6) are obtained using the 'Dormand–Prince 8(5,3)' algorithm. However, for triangular fast excitation and single-harmonic base excitation, closed-form analytical solutions are obtained. Analytically obtained transmissibility plots of the on–off isolator without and with triangular fast excitation are shown in Fig. 6. In the same figure, analytical results are compared with that obtained from the direct numerical integration of equation of motion. Transmissibility curve of an ideal sky-hook damper is also shown for comparison. From Fig. 6, it is observed that by proper choice of the strength of fast excitation substantial performance gain may be obtained over the on–off isolator without fast excitation and even the ideal sky-hook isolator. Performance can be improved continuously over a wide frequency range by increasing the fast excitation velocity (V in this case). Maximum improvement is observed near the natural frequency. Thus, it is possible to construct a stiffer isolator having natural frequency not much different from the operating range of frequencies. Fig. 7 illustrates the effect of damping parameter h on the isolator performance. From Fig. 7, it is observed that the effect of fast excitation on the isolator performance is pronounced for higher values of h. In fact, fast vibration acts on the system by improving the effective damping characteristics. Frequency responses of the transmissibility characteristics of the system without and with sinusoidal fast excitation are shown in Figs. 8 and 9, respectively. Similar characteristics are observed as in the previous case.

It is interesting to compare the analytically obtained effective damping characteristics with that obtained by numerical integration. Effective damping function obtained from direct numerical integration is plotted in Fig. 10. To obtain the figure, relative velocity across the damper and damping force are sampled at the rate of 100/unit time for a total sample period of 100. These

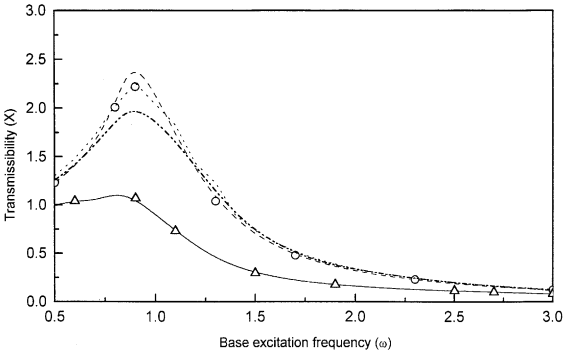

Fig. 6. Transmissibility curves of on–off isolator with and without triangular fast excitation: ——, $V = 1.0$ (analytical); ○, $V = 1.0$ (numerical); ——, $V = 2.5$ (analytical); △, $V = 2.5$ (numerical); ------, without fast excitation, $h = 0.5$; — - - — - -, ideal sky-hook damping.

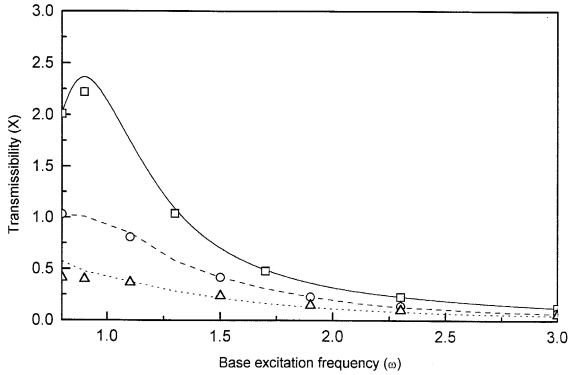

Fig. 7. Effect of damping factor h on transmissibility curves: ——, $h = 0.5$ (analytical); – – –, $h = 1.0$ (analytical); -------, $h = 1.5$ (analytical); □, $h = 0.5$ (numerical); ○, $h = 1.0$ (numerical); △, $h = 1.5$ (numerical). $V = 1$.

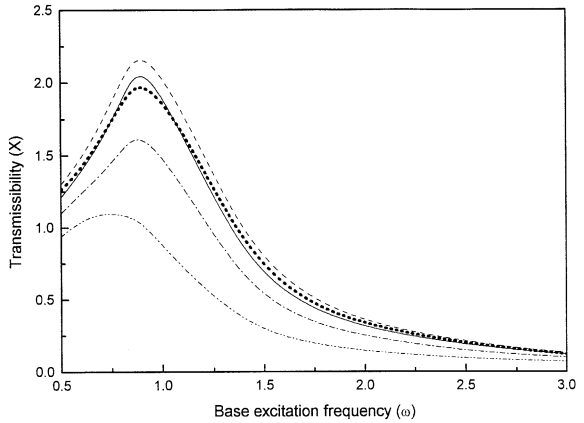

Fig. 8. Transmissibility plots with and without fast excitation. $h = 0.5$: ●●●●, ideal sky-hook; - - - -, on–off without fast excitation; ——, on–off with fast excitation ($q\Omega = 2$); - · - · -, on–off with fast excitation ($q\Omega = 3$); – - – - – - –, on–off with fast excitation ($q\Omega = 4$).

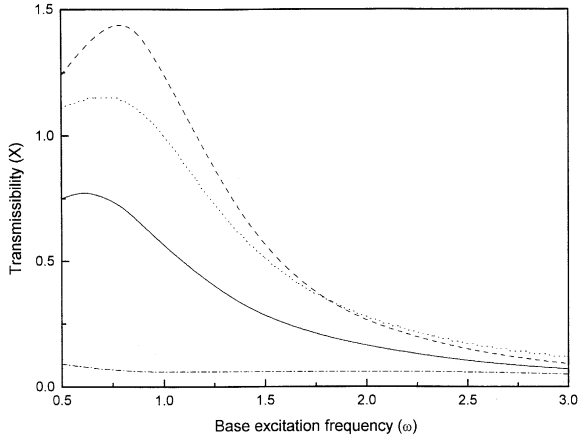

Fig. 9. Transmissibility plots with and without harmonic fast excitation. $h = 1.0$: ····· , ideal sky-hook isolator; - - - -, on–off isolator; ——, on–off with fast excitation ($q\Omega = 2.0$); – - – - –, on–off with fast excitation ($q\Omega = 3.0$).

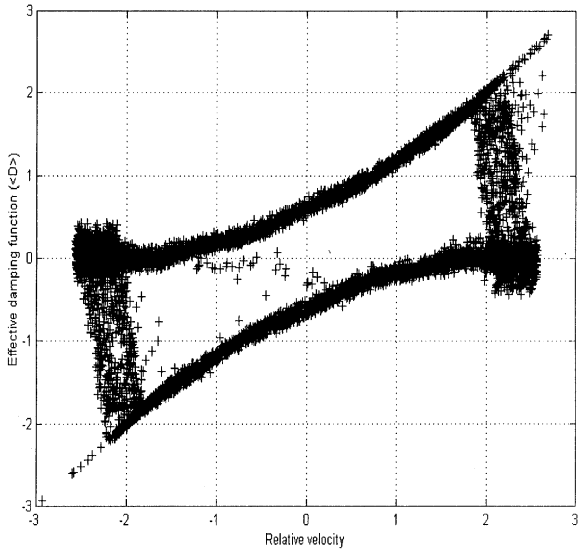

Fig. 10. Numerically simulated effective damping function for sinusoidal fast excitation. $h = 1.0,\ q = 0.002, \Omega = 1000,$ $\omega = 2.5$.

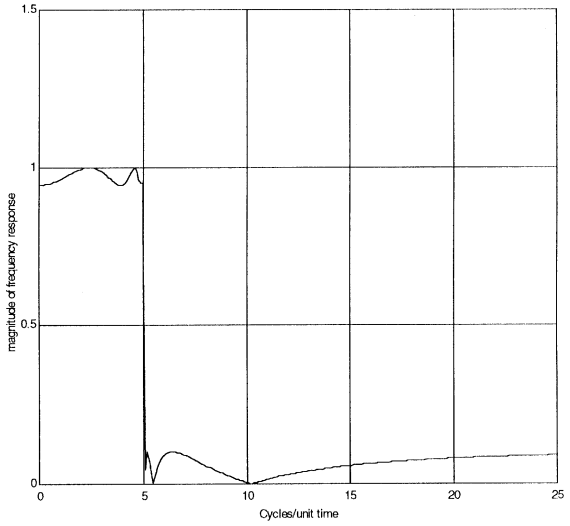

Fig. 11. Frequency response of the elliptical low-pass filter.

signals are subsequently processed through a low-pass elliptical filter of order 8 having the frequency response as shown in Fig. 11. From Fig. 10, one observes two branches of the effective damping curve; the upper curve is for positive absolute velocity and the lower one for negative absolute velocity. Comparing Figs. 4(a) and 10, one finds good qualitative as well as quantitative agreements (for the sake of clarity Figs. 4 and 10 are not superimposed) between the analytical and numerical effective damping characteristics. The scatter of the numerical data in Fig. 10 should not surprise one. As the effective damping plot is constructed after filtering (low-

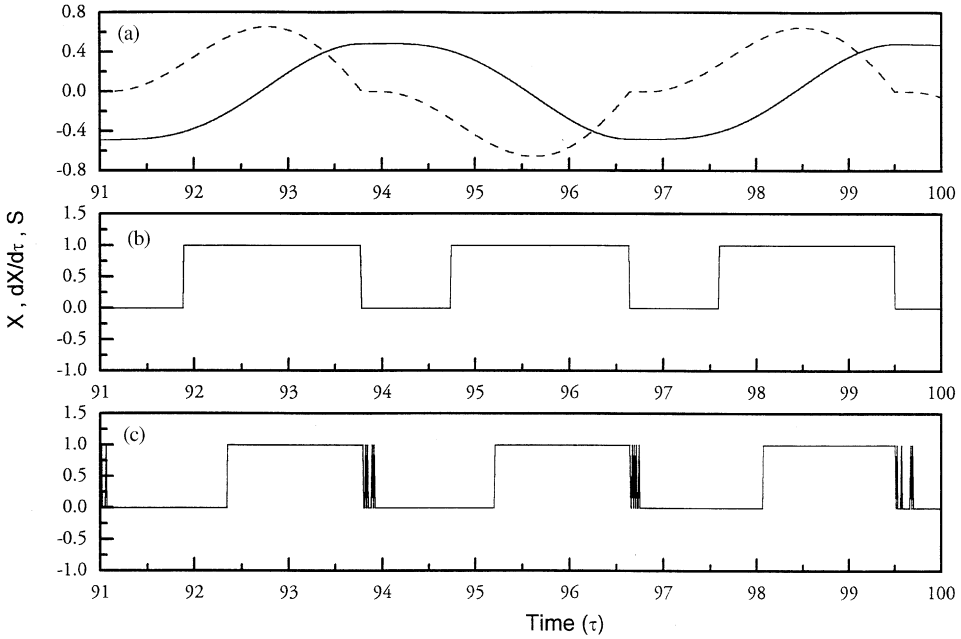

Fig. 12. Time history of response and the switch value for absolute control. (a) Time history of displacement and absolute velocity with fast excitation: ——, displacement; - - - - -, absolute velocity. (b) Time history of switch value without fast excitation. (c) Time history of switch value with fast excitation: $h = 1.0$, $\omega = 1.1$, $q = 0.002$, $\Omega = 1000$.

pass) the signals generated by stimulating the full model (Eq. (6)), there are still some high-frequency components present. Though the high-frequency part causes the data to scatter, one is only interested in the average damper force. A better filter characteristic might have minimized the data scatter. In Fig. 10, one may note the presence of vertical transition branches, which are missing from Fig. 4. This is because of the fact that in numerical simulation (possibly also in practice), transition from positive absolute velocity to negative absolute velocity is not always instantaneous. For some parameter values, transition is closely resembling sticking phenomena [1] observed in friction interfaces. This sticking phenomenon is illustrated in Fig. 12(a). Sticking is particularly present in a system either with high value of damping factor h or high amplitude of velocity of fast excitation (equivalent to high effective damping).

Comparisons of the time histories of the switch values S with and without fast excitations are made in Figs. 12(b) and (c). From Fig. 12(c), one observes that besides the low-frequency switching intervals, several high-frequency transitions between the on and off phases are present in a single period of the switch time history. This accounts for the enhanced effective damping characteristics of the system.

4. Theoretical analysis with dynamic friction model

The model of the friction damper considered hitherto is only a simplified steady state representation of more rigorous dynamic models of friction available in literature. One of these

dynamic models is known as the LuGre [9] friction model, where friction force is described as average force of deflection of the asperities (modelled as spring-like elastic bristles) of the frictional interface. The equation of motion of the system illustrated in Fig. 1 is then written as

$$mX^{*''} + k(X^* - X_e^*) + S^*N|X^{*'} - X_e^{*'} - X_f^{*'}|\left[\sigma_0^* y^* + \sigma_1^* \frac{\mathrm{d}y^*}{\mathrm{d}t} + \sigma_2^*(X^{*'} - X_e^{*'} - X_f^{*'})\right] = 0,$$

$$\frac{\mathrm{d}y^*}{\mathrm{d}t} = (X^{*'} - X_e^{*'} - X_f^{*'}) - |X^{*'} - X_e^{*'} - X_f^{*'}|\frac{\sigma_0^* y^*}{\mu}, \tag{32}$$

where

$$S^* = \mathrm{U}[X^{*'}(X^{*'} - X_e^{*'} - X_f^{*'})], \quad \text{with U(.) as Heaviside step function,}$$

In the above equation σ_0^*, σ_1^* and σ_2^* are bristle stiffness, bristle damping and viscous damping coefficients, respectively. S^* is the switch function, N is normal load on the friction joint and μ is coefficient of friction. y^* represents average bristle deflection of the friction interface. Though in the full form of the LuGre friction model the Stribeck effect parameters are also included, it is of no importance in the present study, and hence is excluded form the model. A non-dimensional form of Eq. (32) may be written as

$$\ddot{X} + (X - X_e) + SF_n^*|\dot{X} - \dot{X}_e - \dot{X}_f|\left[\sigma_0 Y^* + \sigma_1 \frac{\mathrm{d}Y^*}{\mathrm{d}\tau} + \sigma_2(\dot{X} - \dot{X}_e - \dot{X}_f)\right] = 0,$$

$$\frac{\mathrm{d}Y^*}{\mathrm{d}\tau} = (\dot{X} - \dot{X}_e - \dot{X}_f) - |\dot{X} - \dot{X}_e - \dot{X}_f|\frac{\sigma_0 Y^*}{\mu}, \tag{33}$$

where

$$F_n^* = \frac{N}{m\omega_n}, \quad Y^* = \frac{y^*}{x_0}, \quad \sigma_0 = \sigma_0^* x_0, \ \ \sigma_1 = \sigma_1^* x_0 \omega_n, \ \ \sigma_2 = \sigma_2^* x_0 \omega_n, \quad S = \mathrm{U}[\dot{X}(\dot{X} - \dot{X}_e - \dot{X}_f)],$$

and other parameters are as defined in Section 2.

Putting $Y = X - X_e - X_f$, Eq. (33) can be rewritten as

$$\ddot{Y} + Y + D = -\ddot{X}_e - \ddot{X}_f - X_f,$$

$$\frac{\mathrm{d}Y^*}{\mathrm{d}\tau} = \dot{Y} - |\dot{Y}|\frac{\sigma_0 Y^*}{\mu}, \tag{34}$$

where

$$D = SF_n^*|\dot{Y}|\left[\sigma_0 Y^* + \sigma_1 \frac{\mathrm{d}Y^*}{\mathrm{d}\tau} + \sigma_2 \dot{Y}\right] = SF_n^*|\dot{Y}|\left[\sigma_0 Y^* + \sigma_1\left(\dot{Y} - |\dot{Y}|\frac{\sigma_0 Y^*}{\mu}\right) + \sigma_2 \dot{Y}\right]$$

and

$$S = \mathrm{U}[(\dot{Y} + \dot{X}_e + \dot{X}_f)(\dot{Y})].$$

4.1. Effective damping for triangular fast excitation

The triangular fast excitation is as illustrated in Fig. 3. According to the MDPM [10], one can split the motion described in Eq. (34) into slow (Y_s, Y_s^*) and fast ($\phi_{1,2}$) components as

$$Y(\tau) = Y_s(\tau) + T_0\phi_1(\tau, T),$$
$$Y^*(\tau) = Y_s^*(\tau) + T_0\phi_2(\tau, T), \tag{35}$$

where

$$T = T_0^{-1}\tau,$$

and

$$\langle \phi_{1,2} \rangle = T_0^{-1}\int_0^{T_0} \phi_{1,2}(\tau, T)\,\mathrm{d}T = 0. \tag{36}$$

From Eq. (35), one obtains

$$\dot{Y}(\tau) = \dot{Y}_s(\tau) + \phi_1' + T_0\dot{\phi}_1, \tag{37}$$

$$\ddot{Y}(\tau) = \ddot{Y}_s(\tau) + \phi_1''T_0^{-1} + 2\dot{\phi}_1' + T_0\ddot{\phi}_1, \tag{38}$$

$$\dot{Y}^*(\tau) = \dot{Y}_s^*(\tau) + \phi_2' + T_0\dot{\phi}_2, \tag{39}$$

where $'$ and $\dot{}$ denote differentiation with respect to T and τ, respectively.

Now putting Eqs. (37)–(39) in Eq. (34), one obtains

$$\phi_1'' = -T_0\{\ddot{Y}_s + 2\dot{\phi}' + Y_s + D + \ddot{X}_e\} - T_0\ddot{X}_f + O(T_0^2), \tag{40a}$$

$$\phi_2' = -\dot{Y}_s^* + \dot{Y}_s + \phi_1' - |\dot{Y}_s + \phi'|\frac{\sigma_0 Y_s^*}{\mu}, \tag{40b}$$

where $'$ denotes differentiation with respect to T.

If fast excitation is strong enough such that

$$T_0\ddot{X}_f \sim O(1) \text{ or higher},$$

the first order form of Eq. (40a) becomes

$$\phi_1'' = -T_0\ddot{X}_f. \tag{41}$$

Integrating Eq. (41) one obtains ϕ_1' as a square wave of amplitude V, as described in Section 3.2. Using this information and Eq. (36), Eqs. (40a) and (40b) are averaged to obtain the slow dynamics of the system as

$$\ddot{Y}_s + Y_s + \langle D(Y_s^*, \dot{Y}_s + \phi_1') \rangle = -\ddot{X}_e, \tag{42a}$$

$$\dot{Y}_s^* = \dot{Y}_s - \langle |\dot{Y}_s + \phi_1'| \rangle \frac{\sigma_0 Y_s^*}{\mu}, \tag{42b}$$

where

$$\langle D \rangle = \left\langle S^p F_n^* |\dot{Y}_s^p| \left[\sigma_0 Y_s^* + \sigma_1\left(\dot{Y}_s^p - |\dot{Y}_s^p|\frac{\sigma_0 Y_s^*}{\mu}\right) + \sigma_2 \dot{Y}_s^p\right]\right\rangle, \tag{43}$$

with

$$S^p = \mathrm{U}[(\dot{Y}_s^p + \dot{X}_e)(\dot{Y}_s^p)],$$

where

$$\dot{Y}_s^p = \dot{Y}_s + \phi_1'.$$

Thus, one obtains

$$\langle D \rangle = 0.5 F_n^* (D_1^+ + D_1^-), \tag{44}$$

with

$$D_1^+ = S^+ F_n^* |\dot{Y}_s^+| \left[\sigma_0 Y_s^* + \sigma_1 \left(\dot{Y}_s^+ - |\dot{Y}_s^+| \frac{\sigma_0 Y_s^*}{\mu} \right) + \sigma_2 \dot{Y}_s^+ \right]$$

and

$$D_1^- = S^- F_n^* |\dot{Y}_s^-| \left[\sigma_0 Y_s^* + \sigma_1 \left(\dot{Y}_s^- - |\dot{Y}_s^-| \frac{\sigma_0 Y_s^*}{\mu} \right) + \sigma_2 \dot{Y}_s^- \right],$$

where

$$S^+ = \mathrm{U}[(\dot{Y}_s^+ + \dot{X}_e)(\dot{Y}_s^+)],$$

$$\dot{Y}_s^+ = \dot{Y}_s + V$$

and

$$S^- = \mathrm{U}[(\dot{Y}_s^- + \dot{X}_e)(\dot{Y}_s^-)],$$

$$\dot{Y}_s^- = \dot{Y}_s - V.$$

Similarly, Eq. (42b) can be written as

$$\varepsilon \dot{\xi} = \dot{Y}_s - \frac{1}{2}[|\dot{Y}_s + V| + |\dot{Y}_s - V|] \frac{\xi}{\mu}, \tag{45}$$

where

$$\xi = \sigma_0 Y_s^* \quad \text{and} \quad \varepsilon = \frac{1}{\sigma_0}.$$

As σ_0 is generally numerically very large, one assumes $\varepsilon \ll 1$, and hence Eq. (45) turns out to be a standard singular perturbation problem. Putting $\varepsilon = 0$ in Eq. (45), one obtains the slow manifold of Eq. (45) as follows:

$$\xi = \frac{2\mu \dot{Y}_s}{|\dot{Y}_s + V| + |\dot{Y}_s - V|}. \tag{46}$$

Using the following time and co-ordinate transformation,

$$\hat{\xi} = \xi - \frac{2\mu \dot{Y}_s}{|\dot{Y}_s + V| + |\dot{Y}_s - V|}$$

and

$$\hat{\tau} = \frac{\tau}{\varepsilon},$$

and considering $\dot{Y}_s$ as constant, one obtains the boundary layer problem describing the fast dynamics as

$$\frac{\mathrm{d}\hat{\xi}}{\mathrm{d}\hat{\tau}} = -\frac{1}{2}\hat{\xi}\left(\frac{|\dot{Y}_s + V|}{\mu} + \frac{|\dot{Y}_s - V|}{\mu}\right). \tag{47}$$

One may observe that the equilibrium point

$$\hat{\xi} = 0$$

of the boundary layer problem (47) is uniformly asymptotically stable for all velocities. Therefore, according to the Tikhonov's theorem, the slow manifold given by Eq. (46) describes steady state dynamics of ξ. Thus, one can write

$$Y_s^* = \left(\frac{1}{\sigma_0}\right)\frac{2\mu\dot{Y}_s}{|\dot{Y}_s + V| + |\dot{Y}_s - V|}. \tag{48}$$

Therefore, using Eqs. (44) and (48), one obtains the effective damping characteristics of the system. As a numerical example, the graphical nature of the effective damping is shown in Fig. 13. As in the case of steady state friction model, the effective damping characteristics for dynamic friction model are also having two branches of curves, each for a particular direction of absolute velocity of the mass. Around lower values of relative velocity (low-frequency part) across the damper, damping is improved and acting against absolute velocity of the mass, and hence a better isolation performance is predicted. At higher relative velocities, unfavourable damping behaviour is observed, and the range of relative velocities corresponding to this unfavourable damping

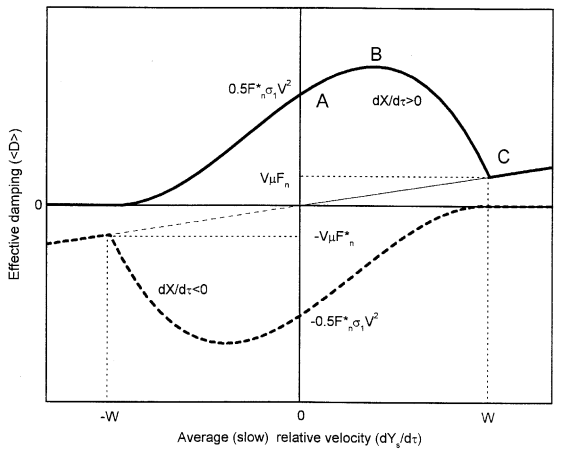

Fig. 13. Effective damping characteristics for the LuGre model of friction with triangular fast vibration: ——, with fast vibration ($\mathrm{d}X/\mathrm{d}\tau > 0$); - - - -, with fast vibration ($\mathrm{d}X/\mathrm{d}\tau < 0$); ——, without fast vibration ($\mathrm{d}X/\mathrm{d}\tau > 0$); – – – –, without fast vibration ($\mathrm{d}X/\mathrm{d}\tau < 0$).

behaviour shifts towards higher velocity with the increasing strength of fast excitation. However, numerical simulations have shown that relative velocity does not reach that value provided proper choice of the strength (here V) of fast excitation is made. The effective damping characteristics with fast vibration may be quantitatively characterized by the damping values of the three points A, B (low-velocity peak in the effective damping plot) and C as illustrated in Fig. 13. The values of the effective damping at those points are expressed as follows:

$$\langle D \rangle_A = 0.5 F_n^* \sigma_1 V^2, \tag{49a}$$

$$\langle D \rangle_B = \frac{F_n^*}{2}\left\{\frac{\mu\Psi}{V}(\Psi + V) + \sigma_1(\Psi + V)^2 - \sigma_1(\Psi + V)^2\frac{\Psi}{V}\right\}, \tag{49b}$$

where Ψ is the relative velocity at the point B and is given by

$$\Psi = \frac{1}{\gamma}\left[1 - \sqrt{1 - \gamma V}\right] \quad \text{with } \gamma = \frac{3\sigma_1}{\mu - \sigma_1 V},$$

and

$$\langle D \rangle_C = V\mu F_n^*. \tag{49c}$$

Obviously the values of $\langle D \rangle_A$ and $\langle D \rangle_C$ increase with the increasing value of normal load, the strength of the fast excitation, frictional properties (σ_1 and μ) of the damper. Both the velocity (low-frequency part of the relative velocity across the damper) and the damping value of the point B, $\langle D \rangle_B$ increase with the strength of fast excitation (V). The change of the co-ordinates of the point B with V is shown in Fig. 14. Therefore, one may improve the effective damping characteristics of the system by increasing the strength of fast excitation.

4.2. Isolator performance for triangular fast excitation

Displacement transmissibility of the system are obtained by numerically simulating equation of motion (4.1.2) for harmonic base excitation, and plotted in Fig. 15. From Fig. 15, it is observed that for weaker fast excitation, there exists a jump resonance in the frequency response. This jump resonance is similar to that obtained in case of soft non-linear oscillators, and associated with the

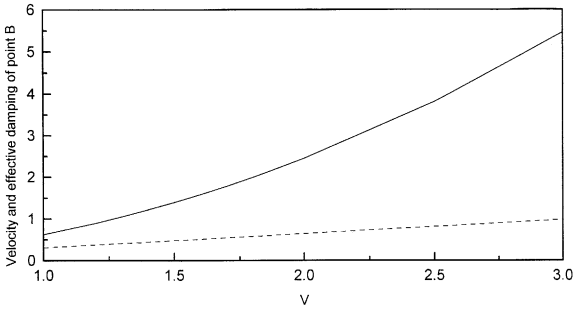

Fig. 14. Variation of the velocity and effective damping of point B with the strength of fast vibration: ----, velocity of the point B; ——, effective damping of point B. $\mu = 0.2$, $F_n^* = 1.0$, $\sigma_1 = 1$, $\sigma_0 = 100$.

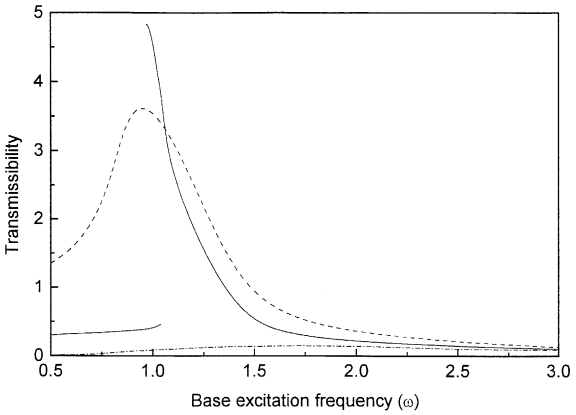

Fig. 15. Displacement transmissibility plot without and with triangular fast vibration. $\sigma_0 = 100$, $\sigma_1 = 1$, $F_n^* = 1$, $\mu = 0.2$. -----, $V = 0$; ——, $V = 1.3$; – - - - –, $V = 1.5$.

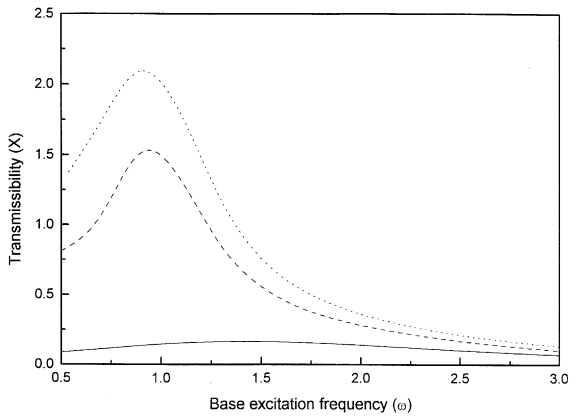

Fig. 16. Transmissibility plot without and with sinusoidal fast excitation considering LuGre friction model. $\sigma_0 = 100$, $\sigma_1 = 1$, $\sigma_2 = 0$, $\mu = 0.5$, $F_n^* = 1$.⋯⋯, without fast excitation; -----, with fast excitation, $q = 0.0015$, $\Omega = 1000$; ——, with fast excitation, $q = 0.002$, $\Omega = 1000$.

'hump' in the effective damping characteristics shown in Fig. 13. However, this undesirable jump resonance is completely removed by increasing the strength of fast excitation.

4.3. Isolator performance for harmonic fast excitation

In this section, direct numerical simulation equation of motion (33) with harmonic base and fast excitation is carried out to plot the transmissibility characteristics. The parameter values of the model are so chosen as to keep the transmissibility characteristics without fast excitation similar to that obtained in case of the steady state Coulomb's friction model. A transmissibility characteristic is shown in Fig. 16. From Fig. 16, it is observed that using fast excitation, substantial improvement is obtained in the transmissibility characteristics.

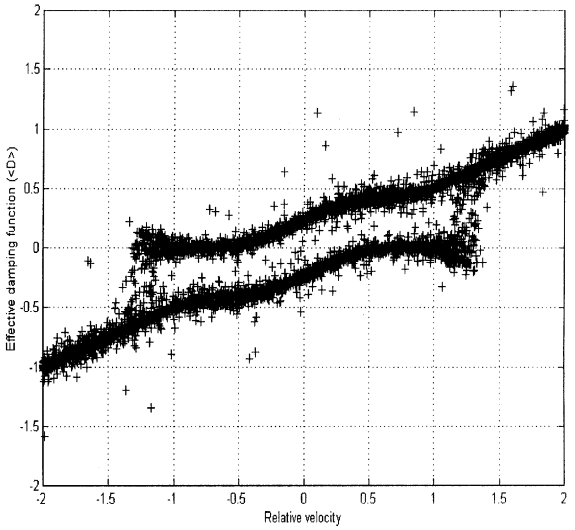

Fig. 17. Numerically simulated effective damping plot with harmonic fast excitation and dynamic friction model. $\sigma_0 = 100,\ \sigma_1 = 1,\ \sigma_2 = 0,\ \mu = 0.5,\ F_n^* = 1,\ q = 0.001,\ \Omega = 1000,\ \omega = 1.4$.

It is also interesting to look into the effective damping plot for harmonic fast excitation. Such a plot is generated and plotted in Fig. 17. The methodology used in plotting Fig. 17 is similar to that used in Section 3.1.

5. Conclusions

An alternative isolator configuration with high-frequency low-amplitude excitation at the base of an on–off friction damper is discussed in this paper. Friction is modelled using the standard Coulomb's friction model and the LuGre friction model. Two different types of fast excitations, namely single-harmonic and triangular wave excitation are considered for theoretical analysis. Analytical expressions are obtained for the effective damping characteristics of the damper under fast excitation, and the performance of the isolators are discussed in light of the effective damper characteristics. It is observed that the effective damper characteristics are improved by increasing the damper parameters as well as the strength of fast excitation. Performance of the isolator is discussed in terms of the displacement transmissibility characteristics. It is shown that the proposed isolator with fast excitation input performs much better than the corresponding isolator without fast excitation input, and with proper choices of the parameters, the proposed isolator performs even better than the ideal sky-hook isolator does.

It is observed from the transmissibility plots that with fast vibration, displacement transmissibility remains very low near the frequency range around the isolator resonance frequency. Thus, it is possible to develop rigid isolators with good transmissibility characteristics. Such configuration of isolators may be suitable for protecting very lightweight and sensitive equipment in situations where fluidic dampers are unsuitable.

Appendix

$$\langle D \rangle = \frac{1}{2\pi} \int_{\theta_1}^{2\pi-\theta_1} (\dot{Z} - q\Omega \cos\theta)\, \mathrm{d}\theta \quad \forall \dot{X}_e + \dot{Z} > 0 \text{ and } |\dot{Z}| \leqslant q\Omega$$
$$= \dot{Z} + \frac{1}{\pi}[q\Omega \sin\theta_1 - \theta_1 \dot{Z}],$$

where

$$\theta_1 = \cos^{-1}\left(\frac{\dot{Z}}{q\Omega}\right),$$

$$\langle D \rangle = \begin{cases} \dfrac{1}{2\pi}\left[\int_0^{\theta_1} (\dot{Z} - q\Omega\cos\theta)\,\mathrm{d}\theta + \int_{2\pi-\theta_1}^{2\pi} (\dot{Z} - q\Omega\cos\theta)\,\mathrm{d}\theta\right] \\ \quad = \dfrac{1}{\pi}[\dot{Z}\theta_1 - q\Omega\sin\theta_1], \\ \quad \forall \dot{X}_e + \dot{Z} < 0 \text{ and } |\dot{Z}| \leqslant q\Omega, \\ \dfrac{1}{2\pi}\int_0^{2\pi} (\dot{Z} - q\Omega\cos\theta)\,\mathrm{d}\theta \\ \quad = \dot{Z}, \\ \quad \forall \dot{X}_e + \dot{Z} > 0 \text{ and } \dot{Z} \geqslant q\Omega, \\ \dfrac{1}{2\pi}\int_0^{2\pi} (\dot{Z} - q\Omega\cos\theta)\,\mathrm{d}\theta \\ \quad = \dot{Z}, \\ \quad \forall \dot{X}_e + \dot{Z} < 0 \text{ and } \dot{Z} \leqslant -q\Omega, \\ 0 \\ \quad \text{otherwise.} \end{cases}$$

References

[1] D. Karnoop, M.J. Crosby, R.A. Harwood, Vibration control using semi-active force generators, *American Society of Mechanical Engineers, Journal of Engineering for Industry* May (1974) 619–626.

[2] D. Karnoop, Design principles of for vibration control using semi-active dampers, *American Society of Mechanical Engineers, Journal of Dynamic Systems, Measurement, and Control* 112 (3) (1990) 448–455.

[3] S. Rakheja, S. Sankar, Vibration and shock isolation performance of a semi-active on off damper, *American Society of Mechanical Engineers, Journal of Vibration, Acoustics, Stress, and Reliability in Design* 107 (1985) 398–403.

[4] H. Yoshida, et al., Sky-hook following control of vehicle using an ER damper, *Proceedings of the Ninth SEAD*, Vol. C14, 1997, pp. 493–502.

[5] A.K. Carter, Transient motion control of passive and semi-active damping for vehicle suspension, Masters Thesis, Virginia Polytechnic Institute and State University, Blacksburg, VA, USA, 1998.

[6] A.A. Ferri, Modelling and analysis of nonlinear sleeve joints of large space structures, *American Institute of Aeronautics, Journal of Spacecraft and Rockets* 25 (1988) 354–360.

[7] H. Yamaguchi, M. Yashima, Y. Hirayama, Vibration reduction and isolation by on-off control of friction force at spring support, *Proceedings of the ASME/DETC 16th Biennial Conference on Mechanical Vibration and Noise*, Sacramento, Vol. VIB-3802, 1997.
[8] A. Nishitani, Y. Nitta, Y. Ikeda, Semi-active variable-friction damper control with simple algorithm, *Proceedings of the American Control Conference*, Chicago, Vol. 1, 2000, pp. 503–507.
[9] C. Canudas, D.E. Wit, H. Olsson, K. Astrom, P. Lischinsky, A new model for control of systems with friction, *IEEE Transactions on Automatic Control* 40 (1995) 419–425.
[10] I.I. Blekhman, *Vibrational Mechanics—Nonlinear Dynamic Effects, General Approach, Applications*, World Scientific, Singapore, 2000.
[11] H. Khalil, *Nonlinear Systems*, 2nd Edition, Macmillan, New York, 1996.
[12] S. Chatterjee, T.K. Singha, S.K. Karmakar, Non-trivial effect of fast vibration on the dynamics of a class of non-linearly damped mechanical systems, *Journal of Sound and Vibration* 260 (4) (2003) 711–730.
[13] J.S. Jensen, Buckling of an elastic beam with added high-frequency excitation, *International Journal of Non-Linear Mechanics* 35 (2) (2000) 217–227.
[14] J.J. Thomsen, Some general effects of strong high-frequency excitation: stiffening, biasing, and smoothening, DCAMM, Technical University of Denmark, Report No. 660, 2001.
[15] M.H. Hansen, Effect of high-frequency excitation on natural frequencies of spinning disks, *Journal of Sound and Vibration* 234 (4) (2000) 577–589.
[16] J.J. Thomsen, D.M. Tcherniak, Chelomei's pendulum explained, *Proceedings of the Royal Society of London A* 457 (2012) (2001) 1889–1913.
[17] J.J. Thomsen, Using fast vibrations to quench friction-induced oscillation, *Journal of Sound and Vibration* 228 (5) (1999) 1079–1102.
[18] J.J. Thomsen, Vibration induced displacement using high-frequency resonators and friction layers, *Proceedings of the IUTAM/IFToMM Symposium on Synthesis of Nonlinear Dynamical Systems—SNDS'98*, Riga, Latvia, August 24–28, 1998, Kluwer Academic Press, Dordrecht, 1999.
[19] J.S. Jensen, Fluid transport due to nonlinear fluid–structure interaction, *Journal of Fluids and Structures* 11 (1997) 327–344.
[20] S. Chatterjee, A.K. Mallik, A. Ghosh, Periodic response of piecewise non-linear oscillator under harmonic excitation, *Journal of Sound and Vibration* 191 (1) (1996) 129–144.